JOURNAL OF AIRCRAFT
Vol. 43, No. 4, July–August 2006

# Numerical Simulation of the Effects of Spanwise Blowing on Tip Vortex Formation

Karthikeyan Duraisamy* and James D. Baeder†
*University of Maryland, College Park, Maryland 20742*

DOI: 10.2514/1.19746

**A high resolution computational methodology is developed for the solution of the compressible Reynolds-averaged Navier–Stokes equations. This methodology is used to study the effect of spanwise blowing as a method of tip vortex control. The numerical error is reduced by using high order accurate schemes on appropriately refined meshes. For vortex evolution problems, the equations are solved on multiple overset grids that ensure adequate resolution in an efficient manner. Reliable validation of the mean flowfield for the baseline and control configurations is obtained by adding a simple correction to the production term in the Spalart–Allmaras turbulence model. A detailed study of the underlying physics of the effects of spanwise blowing is presented.**

## Introduction

THE vortex sheet generated behind an airplane wing or a helicopter rotor rolls up to form a concentrated region of vorticity near the tip region. Within a few chord lengths downstream of the trailing edge, a coherent vortex is observed. In airplane wakes, this region of strong rotational flow typically persists long enough to pose a hazard to other aircraft. In helicopters, under a variety of flight conditions, the rotor blades pass through the proximity of the tip vortices that are trailed from preceding blades. This has been identified as a significant source of noise and vibration. Hence there is a huge incentive in research towards mitigation of the strength and modification of the structure of tip vortices.

Although the study of tip vortex flowfields has been an extremely active area of research over the past century in the form of analytical, experimental, and computational studies, comprehensive understanding of the intricate details of the flow physics is more qualitative than quantitative. The broad objective of this work is to develop a reliable numerical methodology that can help in understanding the process of vortex formation, roll up and evolution. Once a level of confidence is established in the accuracy of the methodology, it is used in examining the physics of vortex formation and roll up and in the evaluation of the effects of spanwise blowing on vortex formation and evolution.

## Background

### Flow Physics

The physics of the flow is extremely complex in the near-field region of the wing tip since the process is largely turbulent (under flight conditions, the chord based Reynolds numbers for typical airplanes and helicopters can be expected to be in the range of $10^6$–$10^7$) and highly three dimensional. The pressure difference between the upper and lower surfaces of the wing induces a strong cross flow and the associated boundary layer tends to separate (separation is of a secondary nature) once the driving pressure gradient weakens on the top surface [1]. In addition, a weaker secondary vortex of opposite sense (to the tip vortex) has also been observed [2]. These structures continue to evolve on the upper surface of the wing and are ultimately convected downstream of the trailing edge. The presence of such structures with disparate length scales and the associated large gradients in the flow properties complicates any theoretical/experimental/computational attempts to study tip vortices.

In addition, many studies on wing tip vortices [1–4] have reported largely reduced turbulence levels in the vortical core. This has been attributed to the near-solid body rotation that exists in the core. Analytical studies, based on linear stability of isolated vortices ([3] and references therein), have also supported this argument by showing the damping of imposed small disturbances in the core. The decay rate appears to be primarily governed by the relative magnitudes of the axial and tangential velocities that exist in the vortical core [4,5] and in cases with small axial velocities (in relation to the tangential velocities), the major diffusion mechanism is laminar rather than turbulent.

### Level of Modeling

It has been well established that direct [6] and even large eddy simulations (LES) [7] become prohibitively expensive when applied to wall-bounded flows at high Reynolds numbers. The inherent deficiency of Reynolds-averaged Navier–Stokes (RANS) models is the fact that some of the turbulent scales (especially the large energy containing ones) depend specifically on the geometry and hence cannot be universally modeled unlike the smaller more isotropic scales that are modeled in LES. However, at least in the foreseeable future, the Reynolds-averaged Navier–Stokes (RANS) equations represent the highest level of fluid-dynamic approximation that can be applied in the numerical simulation of tip vortex flows at flight Reynolds numbers and will hence be utilized in the present study. Although the RANS equations cannot be expected to exactly represent the intricate details of the flowfield as described in the previous paragraphs, as will be shown, validation of the mean flow quantities can be achieved to reasonable accuracy along with extremely good qualitative insight into the flow physics.

### Numerical Issues

Even if one assumes that the governing equations exactly model the physical phenomena, numerical solution is bound to generate errors. In the case of time dependent partial differential equations like the Euler and Navier–Stokes equations, discretization errors can be viewed (in a linear sense) as arising from *numerical dispersion* and *numerical dissipation* [8]. Numerical dispersion causes waves of different wavelengths to propagate at different speeds and can result in spurious oscillations in high-gradient regions. Numerical dissipation acts as an artificial diffusion mechanism and is

Presented as Paper 4726 at the 23rd AIAA Applied Aerodynamics Conference, Toronto, Ontario, 6–9 June 2005; received 29 August 2005; revision received 1 November 2005; accepted for publication 23 November 2005. 

*Research Scientist, Department of Aerospace Engineering.
†Associate Professor, Department of Aerospace Engineering.

the primary factor that causes inaccuracy in most tip vortex calculations. Unlike nonlinear features like shocks, tip vortices have no resteepening mechanisms and hence artificial decay of the vortex will result in an irrecoverable loss of information. Typically, the use of high order accurate schemes [9,10] is essential to reduce numerical errors in tip vortex simulations. Wake et al. [11] present a detailed analysis of the accuracy of up to ninth order upwind schemes in idealized tip vortex simulations. It is reported that at least 10 points are required along the vortex core (in the cross-stream direction) to minimize the inviscid discretization error. Additionally, nonorthogonality of the mesh system with the vortex axis can impose severe restrictions on the aspect ratio of the cells. To approach the theoretical order of accuracy, the spatial mesh points should be distributed smooth manner with mild stretching ratios [12].

## Previous Work

### Numerical Simulations

Numerical simulation of flow over fixed and rotary wings has been an extremely active area of research over the past 20 years. While there have been many attempts in explicitly addressing grid requirements and numerical dissipation ([11–17]), the following survey (though not all encompassing) concentrates only on those computational works that present validations of tip vortex structure with experiments.

Mansour [18] used the RANS equations to study the transonic flowfield of a swept wing. Though the vortex roll up in the tip region was observed, the grid resolution and numerical accuracy was insufficient to achieve good comparison with experiments. Srinivasan et al. [19] performed a RANS study of the effects of wing planform and tip shape on vortex roll up using the ARC3D code with a Baldwin–Lomax turbulence model. When compared with experiments, the qualitative features showed good agreement, but surface pressures near the wing tip showed poor comparison.

Dacles-Mariani et al. [20] validated the experiments of Chow et al. [1] using a RANS formulation with the Baldwin–Barth turbulence model. They studied the effects of numerical schemes, grid requirements, and turbulence model modifications in resolving the vortex formation and roll up. They were able to demonstrate that using 15 points per vortex core diameter, fifth order spatial accuracy for inviscid terms and a modification of the turbulence model, the mean flow characteristics could be reasonably captured. It was, however, concluded that the use of isotropic turbulence closure could be deficient in accurately representing the turbulence field.

Lockard and Morris [21] solved the inviscid Euler equations using a fourth order central differencing scheme to validate the measurements of Devenport et al. [2]. Even with the use of a $2 \times 10^6$ grid point mesh, the vortex was found to diffuse rapidly. The core size was found to grow to more than 2 times the experimental value within a few chord lengths of evolution. The disagreement was attributed to numerical dissipation and also to the inviscid approximation.

Spall [22] conducted an inviscid simulation of the aforementioned test case of Devenport et al. using a second order accurate scheme with highly refined meshes in the tip vortex region. The peak swirl velocity was overpredicted and the core radius was smaller compared with the experiments. The numerical diffusion was found to be small in that the peak swirl velocity diminished by 15% over a distance of 10 chord lengths.

Egolf et al. [23] present a review of research at the Universal Technologies Research Center on tip vortex simulation. A comprehensive study was made on the numerical diffusion in terms of mesh spacing, mesh alignment, and order of accuracy. For an idealized vortex problem, it is shown that numerical diffusion can be negligible using a ninth order accurate scheme with approximately 12 points in the vortical core. In addition, the mesh points had to be aligned with the vortex axis. However, practical tip vortex simulations using the RANS equations were found to be very dissipative, probably because of the ill effects of the Baldwin–Lomax turbulence model.

### Spanwise Blowing

The effect of spanwise blowing at the wing tip has been experimentally explored by various researchers. Lee et al. [24] studied the flow structure and scaling laws from a low aspect ratio NACA0018 wing in a wind tunnel. The effect of a thin spanwise jet was to virtually extend the wing span, resulting in a slight lift augmentation. In addition, the tip vortex was found to be more diffuse and displaced upward and outboard off the wing tip. Mineck [25] reports experimental and computational results on spanwise blowing on moderate aspect ratio wings at high subsonic Mach numbers. The momentum of the jet was found to be larger than the reduction in the wing drag and the increase in the wing lift due to spanwise blowing was also found to be small. Han and Leishman [26] examined the effect of spanwise blowing on the vortex structure of a helicopter blade in hover. In their test, air was bled at the leading edge of the blade and injected at the tip through a set of 4 circular orifices. Their conception was that this would inject turbulent structures directly into the core of the tip vortex and thus diffuse it. They were able to demonstrate a 50% reduction in swirl velocity within a downstream distance equivalent to 10 chord lengths. Data on the effect on lift and drag coefficients are not currently available, although a profile power penalty is reported. Heyes et al. [27] studied the effect of steady and pulsed spanwise blowing on the trajectory and structure of the tip vortex. They were able to demonstrate a larger core radius, reduced swirl velocities and a heightened axial velocity deficit compared with the case with no blowing. They also propose spanwise pulsed blowing as a means of exciting cooperative instabilities in wakes. In summary, with the use of spanwise blowing, there seem to be very limited prospects on improving the lift to drag ratio, but the potential to reduce the strength of the vortex is promising. This could be extremely beneficial in alleviating the vortex hazard, especially in the case of rotorcraft, where the strength of the returning wake plays a decisive role in determining the overall vibration, noise and performance characteristics.

## Methodology

Computations are performed using the compressible Reynolds-averaged Navier–Stokes (RANS) code OVERTURNS [12]. The inviscid terms are computed using the fifth/seventh order weighted essentially nonoscillatory (WENO) schemes [28] with Roe's flux difference splitting. At the boundaries, one-sided differencing (with no limiting) was implemented. The viscous terms are computed using second/fourth order central differencing.

This code involves a cell-vertex finite volume implementation and hence, in order to maintain higher order accuracy on a stretched mesh, the definitions of the cell areas and volumes have to be consistent with the overall accuracy of the solver [12]. Hence, a high order scheme (the M3 quartic interpolation of Huynh [29]) is used to locate the edges and interfaces of the control volume. A schematic is presented in Fig. 1.

The Spalart–Allmaras [30] (SA) turbulence model is used to close the RANS equations. This model has gained enormous popularity in aerospace computations since it is numerically efficient and was formulated with such applications in mind. Since it is a linear eddy viscosity model, it has the advantage that it is simple, relatively inexpensive and most importantly, numerically stable. However, such models cannot inherently model effects like streamline curvature, flow rotation etc. [31] and have to be *sensitized* to these effects. To force the model to account for the rotation-induced reduction of turbulence levels in the vortical core, a simple correction to the production term suggested by Spalart[‡] and [20] is used. The SA model uses a production term, which in the wake region, reduces to

$$P = c_{b1} S \nu_t \tag{1}$$

Computations were performed with $S = |\omega|$ and $S = |\omega| + 2\min(0, |D| - |\omega|)$, where $|\omega|$ and $|D|$ are the magnitudes of the vorticity vector and strain tensor, respectively. The former was

[‡]Spalart, P., personal communication.

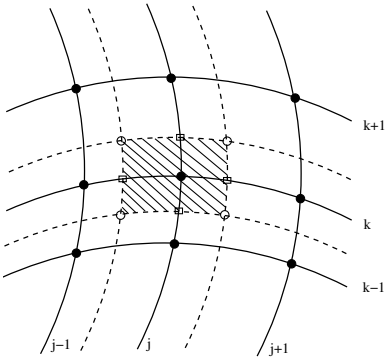


**Fig. 1 2-D schematic of mesh point distribution and control volume definition. Solid circles: mesh points; open circles: edges of control volume. Open squares: interface location for flux calculation.**

suggested in the original paper [30] and the latter version was used in [20], and attempts to suppress the turbulent production in regions (like tip vortices) where the vorticity is much larger than the strain rate. The modification appears to be passive in thin shear layers.

In the spanwise blowing cases, the effect of the jet is modeled as a surface boundary condition. In this procedure, the density ($\rho$) is extrapolated from the interior of the domain to the surface. The contravariant components of the velocity ($U, V, W$) are computed using the Cartesian components of the jet velocity ($\mathbf{Q}_{\text{jet}}$). The pressure ($p$) is then obtained from the normal momentum equation, which is given by

$$p_\xi(\nabla\xi.\nabla\zeta) + p_\eta(\nabla\eta.\nabla\zeta) + p_\zeta(\nabla\zeta.\nabla\zeta) = -\partial_\tau(\rho\mathbf{Q}_{\text{jet}}.\nabla_\zeta) - \rho U\left(\nabla\zeta.\frac{\partial\mathbf{Q}}{\partial\xi}\right) - \rho V\left(\nabla\zeta.\frac{\partial\mathbf{Q}}{\partial\eta}\right) - \rho W\left(\nabla\zeta.\frac{\partial\mathbf{Q}}{\partial\zeta}\right)$$

where, $\xi$, $\eta$, $\zeta$ represent the wraparound, spanwise and wall-normal directions, respectively. For the boundary condition on the turbulence field, two different approaches were implemented at the jet exit:

1) The working variable was set to $\nu_t = 0.002|Q_{\text{jet}}|\delta$, where $\delta$ is the slot thickness. This roughly corresponds to the average eddy viscosity in a turbulent channel at high Reynolds numbers.[§]

2) $\nu_t$ was extrapolated from the interior of the flowfield.

The effect of these two approaches on the mean field was almost identical and the latter was used for all the computations that follow.

## Numerical Validation

In this section, validation studies will be conducted on the vortex formation in the very near field of a fixed wing. The primary objective of this study is to determine the grid and accuracy requirements and to evaluate the fidelity of the turbulence model. The experimental test case corresponds to a 0.69 aspect ratio NACA 0012 rounded tip wing in a $32 \times 48$ in wind tunnel section at $\alpha = 10°$, $\text{Re} = 4.6 \times 10^6$, and $M_\infty = 0.15$. The experiments were conducted by Chow et al. [1] at NASA Ames Research Center. This particular test case was chosen because of the availability of a comprehensive set of measurements in the wake region and on the wing surface. Static pressure, mean velocity and Reynolds stress data are available at select axial planes, starting at a distance of $x/c = 0.591$ ahead of the trailing edge to $x/c = 0.678$ from the trailing edge. Surface pressure measurements are available from a total of 444 pressure taps located in 12 chordwise rows. The flow is tripped at the leading edge so that a fully turbulent assumption is valid.

The baseline grid for this test case was provided by Zilliac.[‖] This grid consists of $115 \times 189 \times 115$ in the streamwise, spanwise, and normal directions, respectively, filling the test section volume exactly. The grid points were redistributed and smoothed for use in this work. Unlike acoustic waves, the tip vortex involves large

[§]Spalart, P., personal communication.

[‖]Zilliac, G., personal communication.

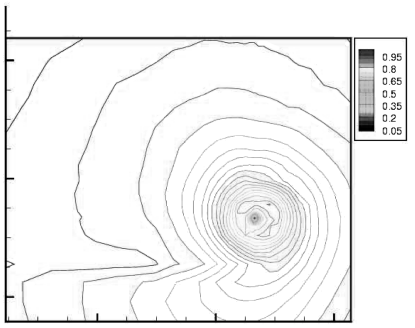


**a) Experiment**

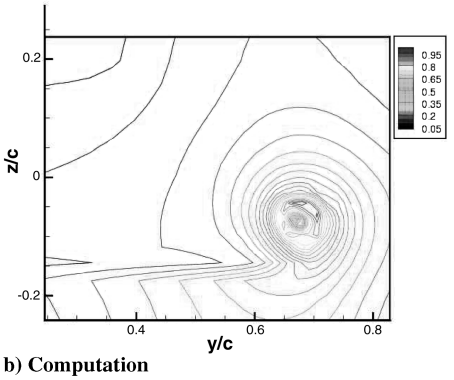


**b) Computation**

**Fig. 2 Crossflow velocity magnitude (normalized by freestream velocity) at $x/c = 0.246$.**

deviations from the free stream and hence care has to be taken to ensure proper boundary treatment. Accordingly, downstream of the test section, the grid was heavily stretched in the streamwise direction and the outflow boundary was extended to 20 chords behind the trailing edge, where characteristic Riemann boundary conditions are applied. This coarse mesh spacing artificially diffuses the vortex downstream of the test section by creating a virtual *buffer zone* so that there are no spurious reflections from the boundary.

To explore and evaluate the effect of numerical and turbulence model errors, various test runs were made. Before the results from all the test runs are presented, the "highest fidelity" numerical result will be compared in detail with experiments. This calculation is performed on the $148 \times 189 \times 115$ grid using the seventh order WENO scheme for inviscid discretization with the rotational correction added to the turbulence model. Subsequently, the other test runs will be compared. For all the results presented, *the origin of the coordinate system is assumed to be at the trailing edge of the wing at the root section*.

Figure 2 compares the contours of the computed swirl velocity $\sqrt{v^2 + w^2}$ along a sample axial plane at $0.246c$ downstream of the trailing edge. To ensure a one-to-one comparison, the computed solution is interpolated on to the experimental data locations before the contours are plotted. Qualitatively and quantitatively, the computed results are similar to that of the experiments. Figure 3 shows the vertical velocity ($w$) along a horizontal (spanwise) line passing through the center of the vortical core. Again, the computed velocity profiles match well with experiments, except at the $x/c = -0.296$ station, where the sharp negative peak is not captured. Figure 4 shows the evolution of the peak magnitudes of the axial velocity $u$, vertical velocity $w$, and total velocity $\sqrt{u^2 + v^2 + w^2}$ with downstream distance. A slight under prediction of the axial and total velocities and an over prediction of the swirl velocity is observed.

Figure 5 shows the pressure distribution on the wing surface. At an inboard section ($y/c = 0.5$) the pressure distribution closely resembles that of a 2-D airfoil. Very close to the tip, a second suction peak appears near the trailing edge, which is a consequence of the tip vortex rolling up on the wing surface. Traversing along the tip

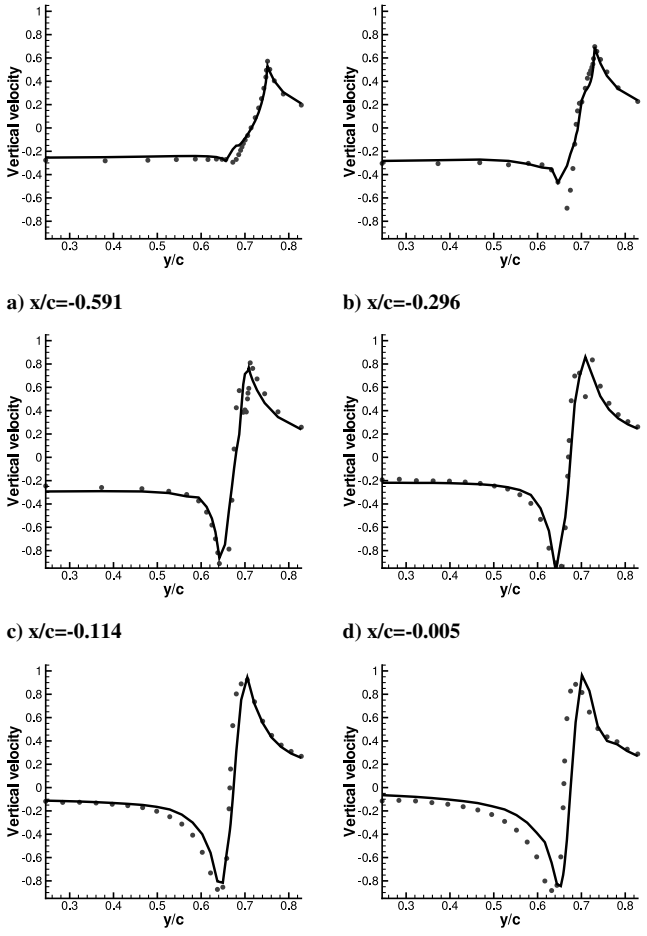


a) x/c=-0.591 b) x/c=-0.296

c) x/c=-0.114 d) x/c=-0.005

e) x/c=0.246 f) x/c=0.678

**Fig. 3 Vertical velocity ($w/U_\infty$) along a horizontal cut through vortex core.**

surface ($0 \leq \gamma \leq 90°$ corresponds to the position on the rounded tip with $\gamma = 0°$ corresponding to the end of the 2-D section and $\gamma = 90°$ corresponding to the camber line), the suction peak near the leading edge is seen to reduce and the pressure at the top and bottom surfaces gradually equalize. The good agreement of the computed results with the experiment is a direct consequence of correctly representing the strength of the evolving tip vortex.

Although the mean flow velocities and surface pressures show good comparisons with the measurements, the computed static pressure and the Reynolds stresses in the vortical core showed considerable error. As reasoned by [20], most of this can be directly attributed to the inaccuracies of the turbulence modeling. These results are discussed in more detail (for instance, the static pressure in the center of the core showed up to 23% *error* and the Reynolds stresses showed a distinct phase lag) in [12]. The present work, however, is an attempt at ascertaining the capabilities of the methodology to quantitatively predict the mean flowfield and to determine the fidelity of the computed physics of formation and roll up.

Further studies in grid convergence, turbulence model effects, and inviscid discretization are reported in [12]. To summarize, with a fifth or higher order WENO discretization, 10–15 points were required along the vortex core in order to achieve the aforementioned accuracy levels. In addition, the use of the rotational correction to the turbulence model was found to be imperative to achieve reasonable predictions.

## Physics of Vortex Formation

As mentioned earlier, the qualitative features of vortex formation and roll up corresponded closely to the experimentally observed flow

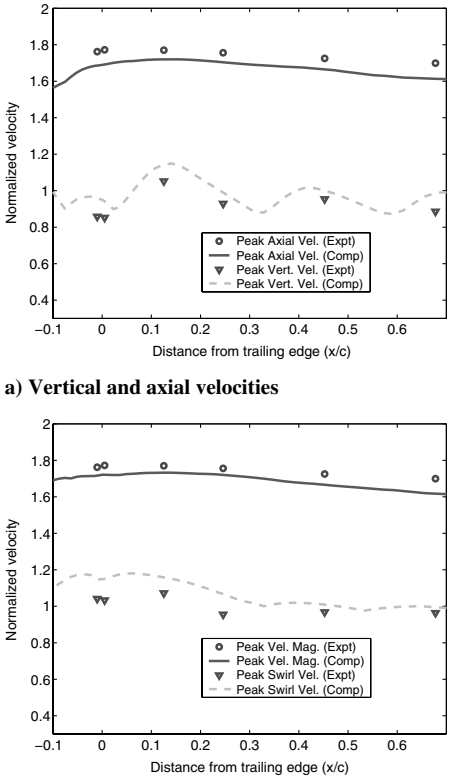


a) Vertical and axial velocities




b) Swirl and total velocities

**Fig. 4 Evolution characteristics of the tip vortex.**

physics. The fine resolution of the computation allows one to analyze the flow in great detail. Figure 6a shows the axial vorticity magnitude along a streamwise section of the wing. A very thin attached boundary layer is observed on the pressure (lower) surface, indicating crossflow. This boundary layer acts as a *feeding sheet* of vorticity and begins to thicken as it crosses the mean chord line since the driving pressure gradient begins to weaken. As marked in the figure, the boundary layer subsequently separates and the feeding sheet lifts off the surface. This feeding sheet then rolls up under the action of is own induced velocity and the prevailing adverse pressure gradient tapers off as one approaches the inboard section of the wing.

The crossflow velocity at the bottom edge of the vortex core induces a near-wall flow on the top surface (the associated boundary layer is evidenced by the blue patch of negative vorticity) in the outboard direction. Closer to the tip, this region is affected by the velocities induced by the feeding sheet and ultimately thickens in extent, appearing as a secondary vortical region that counter-rotates with the evolving tip vortex.

These primary and secondary structures continue to evolve on the surface until the trailing edge is reached. Off the trailing edge, this counter-rotating patch is ingested by the tip vortex as shown in Fig. 6b. The presence of a secondary vortex have been confirmed in the experiment as well as a few others such as Devenport et al. [2], Martin et al. [32]. The interaction of the secondary vortex with the primary vortex severely strains the primary vortex such that the core appears to be elliptical very near to the trailing edge. This explains the apparent "oscillations" in the evolution of the peak vertical and swirl velocities in Fig. 4. A more detailed inspection of the flow very close to the trailing edge reveals the presence of a tertiary vortex which co-rotates with the primary tip vortex. This tertiary vortex is smaller and much weaker compared with the secondary vortex and is located approximately in between the secondary vortex and the feeding sheet.

## Simulation of Spanwise Blowing

### Test Conditions

The test case chosen for this study corresponds to that of the wind

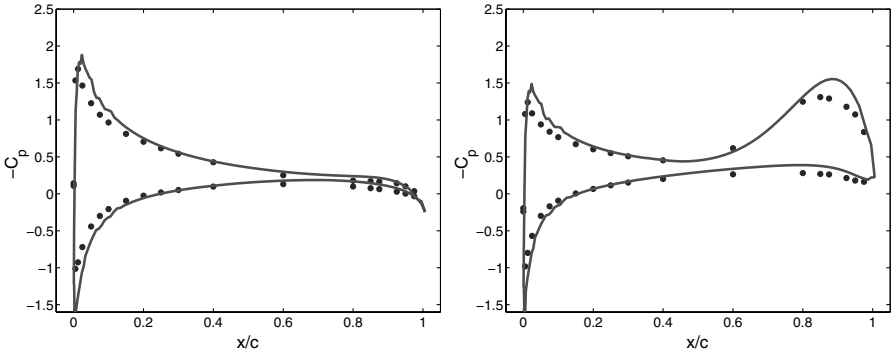


**a) y/c=0.500** **b) y/c=0.667**

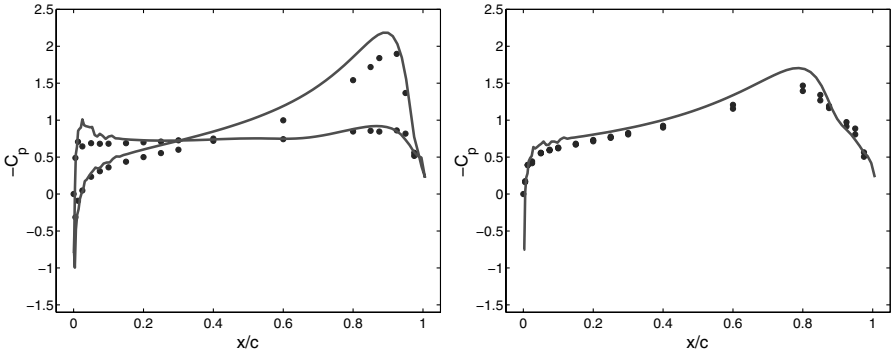


**c) γ=45°** **d) γ=90°**

**Fig. 5 Pressure distribution on wing surface. (Circles: experiment; lines: computation.)**

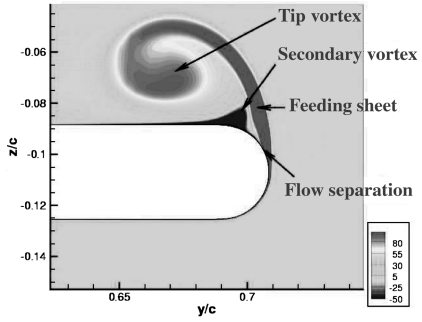


**a) Computed axial vorticity magnitudes at a section *x/c* = –0.15 from the trailing edge. (Positive vorticity is in the anti-clockwise sense)**

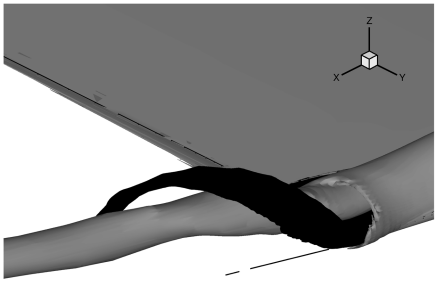


**b) Iso-surfaces of axial vorticity ($\omega_x$) near trailing edge. Light surfaces: $\omega_x$ = +50, Dark surfaces: $\omega_x$ = –10. Vorticity is normalized by free-stream velocity and chord**

**Fig. 6 Physics of vortex formation.**

tunnel experiments conducted by Heyes et al. [27]. The relevant geometry and flow parameters for the half-span wing are given in Table 1. In the experiment, provisions were made to supply compressed air to the tip via a plenum chamber located near the half-span location of the wing. The air exits along an elongated spanwise slot as shown in Fig. 7. As shown in Fig. 7b, the slot geometry is characterized by the length of the slot $L$, the thickness $\delta$, and the jet angle $\theta_{\text{jet}}$. The rate of blowing is characterized by the mass blowing coefficient, which is given by

$$C_\mu = \frac{\hat{m}}{\rho_\infty U_\infty 2bc} \tag{2}$$

where, $\hat{m}$ is the integrated mass rate through the slot and $b$, $c$ are the half-span and wing chord, respectively (in this case, $b = c = 150$ mm).

### Grids Used

The computations in the previous section were focused on the near field. To accurately resolve the vortex evolution many chord lengths downstream, a single structured mesh will be highly inefficient since the clustering of grid points in the cross-stream direction will have to extend to the grid boundaries. To avoid this and also to ensure equal spaced grid points (in the cross-stream direction), an overset grid is placed approximately in the region of the wake where the tip vortex is expected to be present. Figure 8a shows streamwise planes of the main and overset grids. The dimensions of the main grid are $227 \times 100 \times 115$ in the streamwise, spanwise, and normal directions, respectively. The far field is at a distance of 25 chord lengths from the surface. The overset grid has 199 axial planes of size $133 \times 133$. The cross-stream grid spacing is $0.0075c$, assuring at least 10 points per vortex core length. This grid spans an axial distance of $0.25 \leq x/c \leq 15.25$ behind the trailing edge. As shown in Fig. 8b, the main wing mesh (of C-O topology) is made such that a fine resolution is achieved in the regions of vortex formation. Also, in order to reduce

**Table 1 Test conditions for vortex evolution**

| Airfoil section | NACA 0012 |
|---|---|
| Tip shape | Rounded (circular) |
| Chord length (c) | 0.15 m |
| Aspect ratio | 1.0 |
| Mach number | 0.1 |
| Chord Reynolds number | $2.2 \times 10^5$ |
| Angle of attack | 7.5° |

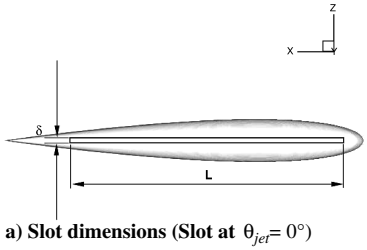


**a) Slot dimensions (Slot at $\theta_{jet}$= 0°)**

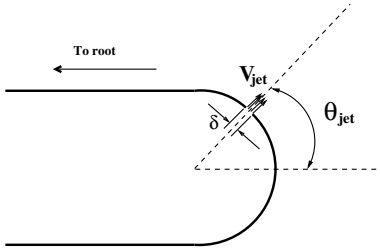


**b) Slot angle**

**Fig. 7 Spanwise blowing slot geometry.**

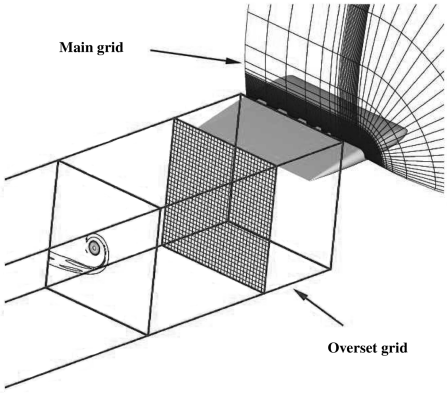


**a) Use of overset grid to resolve the evolving tip vortex**

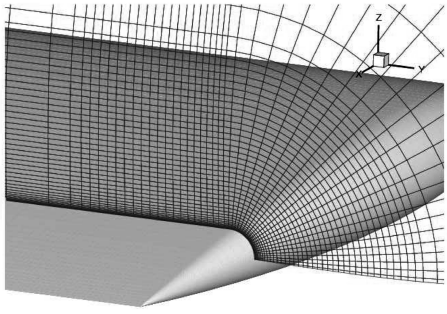


**b) Sample section showing mesh clustering in the region of vortex formation**

**Fig. 8 Grid system used in the blowing case simulation (every other grid point shown).**

interpolation errors across the meshes, the cell sizes of both meshes are approximately matched in the interfacial region of interest. Further, grid clustering ensured at least 12 points across the slot thickness and 85 points across the length. The baseline and control case C1 (Table 2) computations were repeated on an alternate grid with 24 points across the slot thickness and the resulting peak swirl and axial velocity magnitudes were found to differ only by <3%. Hence, the following results are assumed to be grid converged. Modeling the flow in the plenum chamber and the other internal details of the jet flow will prove to be extremely complicated and expensive and hence, the jet exit is modeled as a surface boundary condition as described earlier.

A key difference between the experiment (in which the wind tunnel walls were 2 chord lengths away from the wing surface) and the simulation is that the latter assumes the wing to be in freestream. (The root plane was treated as an inviscid wall.) This was done for ease of grid generation. As will be seen, comparison of the computed vortex velocity profile with the experimental results suggest that the details of the vortex formation are not different. The following results use the 7th order WENO differencing for inviscid fluxes. The Spalart Allmaras turbulence model with rotational correction is used for the RANS closure.

### Baseline Case Validation

For the case with no blowing, Fig. 9 compares the computed vertical and axial velocities on a horizontal line passing through the vortex center at an axial plane that is 1 chord downstream of the trailing edge. The vertical velocity is seen to be accurately represented while the axial velocity defect is slightly under predicted. The defect in axial velocity is a consequence of the low Reynolds number, implying larger viscous deceleration compared with the previous test case. Velocity profile measurements are not available further downstream, however, the computed baseline and blowing vortex evolution results will be compared with each other in the following section.

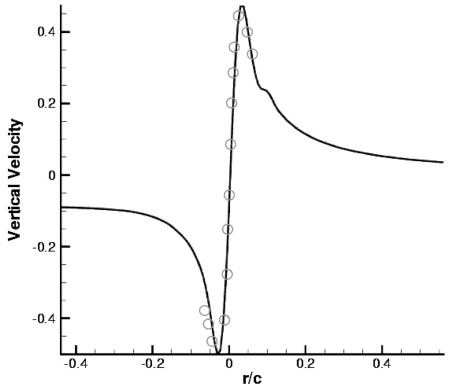


**a) Vertical velocity ($w/U_\infty$)**

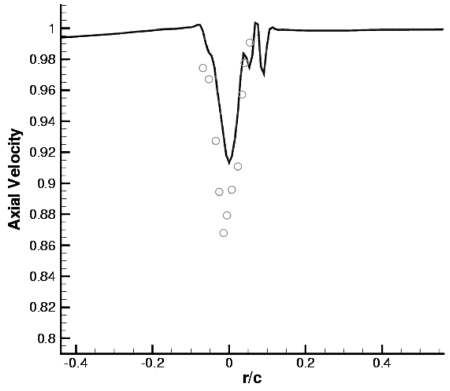


**b) Axial velocity ($u/U_\infty$)**

**Fig. 9 Comparison of computed velocity profile (line) with experiment (circles) at $x/c = 1.0$.**

**Table 2 Comparison of different spanwise blowing cases. For all cases, the slit ends at $x/c = -0.17$ from the trailing edge**

| Case | $\delta/c$ | $L/c$ | $\theta_{\text{jet}}$ | $U_{\text{jet}}/U_\infty$ | $C_\mu$ | $C_L$ | $C_D$ | $L/D$ |
|---|---|---|---|---|---|---|---|---|
| Baseline | —— | —— | —— | —— | —— | 0.3398 | 0.03094 | 10.98 |
| C1 | 1/150 | 0.8 | 0 | 0.866 | 0.00108 | 0.3542 | 0.0327 | 10.83 |
| C2 | 1/150 | 0.8 | 0 | 0.375 | 0.00047 | 0.3465 | 0.0315 | 11.00 |
| C3 | 1/150 | 0.8 | 0 | 0.188 | 0.00024 | 0.3431 | 0.0311 | 11.03 |
| C4 | 1/150 | 0.8 | 15 | 0.866 | 0.00110 | 0.3538 | 0.0325 | 10.89 |
| C5 | 1/150 | 0.8 | −15 | 0.866 | 0.00110 | 0.3539 | 0.0326 | 10.83 |

**Blowing Case Validation and Flow Physics**

The different spanwise blowing simulations that were performed are detailed in Table 2. Of these, C1 corresponds to an experimentally tested case and velocity measurements are available one chord downstream of the trailing edge.

Figure 10 compares the experimental measurements with the computed vertical and axial velocities along a horizontal line passing through the vortex center one chord downstream of the trailing edge. Akin to the baseline case (Fig. 9), the computed velocities agree well with the experimental measurements.

The vortex structure at two downstream locations in the blowing case is compared with the baseline calculations in Fig. 11. At $x/c = 1.0$, a reduced swirl velocity and a heightened axial velocity deficit is observed. The disruption of the crossflow sweeping across the wing tip caused by the spanwise jet results in weaker swirl velocities. Further, as will be explained, the spanwise blowing introduces turbulence directly into the vortical core and this results in strong decelerating forces, causing a larger axial momentum deficit compared with the baseline case.

Some insight can be obtained from Batchelor's simplistic analysis of axial flow in an isolated axisymmetric trailing vortex [33]. Assuming small axial gradients (compared with radial gradients), small radial velocity [compared with axial ($V_a$) and swirl velocities ($V_\theta$)] and a viscous head loss $\Delta H$ to an otherwise inviscid flow, the axial velocity is given by

$$V_a^2 = U_\infty^2 + \int_r^\infty \frac{\Gamma}{2\pi^2 r^2}\frac{\partial \Gamma}{\partial r} dr - 2\Delta H$$

where the circulation is defined by $\Gamma = 2\pi r V_\theta$. Assuming a monotone nondecreasing circulation (which is the case in the flow of our interest), one should expect an axial velocity *excess* for inviscid flow. For viscous flows, the presence of the loss of head competes with the inviscid acceleration mechanism. In the case of large Reynolds numbers and high angles of attack, the inviscid mechanism wins out and an axial velocity excess has been reported in some near-field experiments (for instance, the results in the previous section). Under typically moderate angles of attack, the pressure losses are usually high enough and the majority of experiments have reported axial velocity deficits. In the present case, the combination of the low Reynolds number and the presence of increased turbulence activity causes the large deficit in axial velocity.

The heightened axial velocity deficit will result in radial transport of angular momentum [34], and can thus be expected to diminish the swirl velocity at a larger rate compared with the baseline case. In addition, as opposed to the baseline case, the large axial velocity deficit in the control case at $x/c = 1.0$ would result in a highly unstable configuration according to the linear stability theory of isolated axisymmetric vortices [35].

Figure 12 compares the evolution of the vortex properties for the baseline and blowing cases. The peak swirl velocity is seen to be lower for the blowing case initially and is also seen to decay at a more rapid rate. The heightened axial velocity deficit near the trailing edge is seen to taper off more rapidly compared with the baseline case, but the defect spreads over a much larger area as was observed earlier in Fig. 11.

The turbulence generated by the jet predominantly arises from the counter-rotating vortex pair that exists at the jet exit as schematized in Fig. 13. The physical mechanism of spanwise blowing is illustrated in Fig. 14, in which axial vorticity contours are shown along various streamwise sections. As seen in Fig. 14a, a counter-rotating vortex pair is formed at the jet exit. In this case, the upper vortex (CWJ) is in the positive sense (anticlockwise) and co-rotates with the eventual tip vortex and the lower (CCWJ) one is in the "negative" sense. The presence of both these vortices is seen to disrupt the feeding sheet of vorticity. These vortices are formed (as schematized in Fig. 13) by the roll up of the vortex sheets at the top and bottom of the jet face. Figure 14b shows that the lower vortex is convected much faster to the top surface of the wing since it is not *shielded* from the crossflow. The slower convection of the upper vortex also makes it roll up faster. As seen from Fig. 14c, by the quarter-chord location, the upper vortex entrains vorticity from the feeding sheet and slowly develops into the tip vortex. The presence and strength of the tip vortex results in a secondary counter-rotating region of vorticity (SV), similar to that seen in the vortex formation studies. As the tip vortex evolves (Figs. 14c and 14d), entraining vorticity from the feeding sheet and the CWJ, its "edges" are seen to interact with the CCWJ. As a result, the (positive) vortex strength is weakened. The interaction with the CWJ and the SV also tends to "lift" the evolving tip vortex off the surface as seen in Fig. 14e.

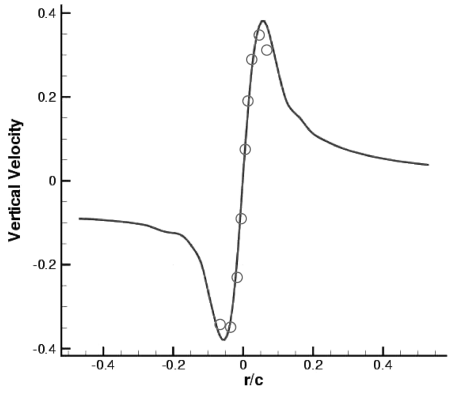


**a) Vertical velocity ($w/U_\infty$)**

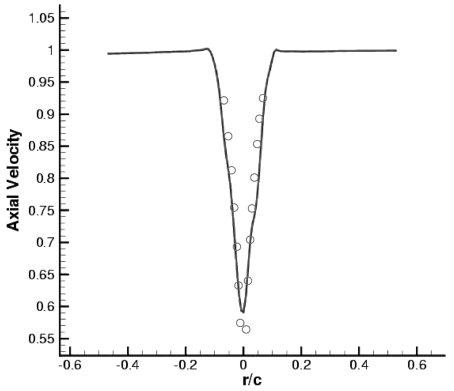


**b) Axial velocity ($u/U_\infty$)**

**Fig. 10 Comparison of computed velocity profile (line) with experiment (circles) at $x/c = 1.0$ for blowing case C1 ($C_\mu = 0.001,08$).**

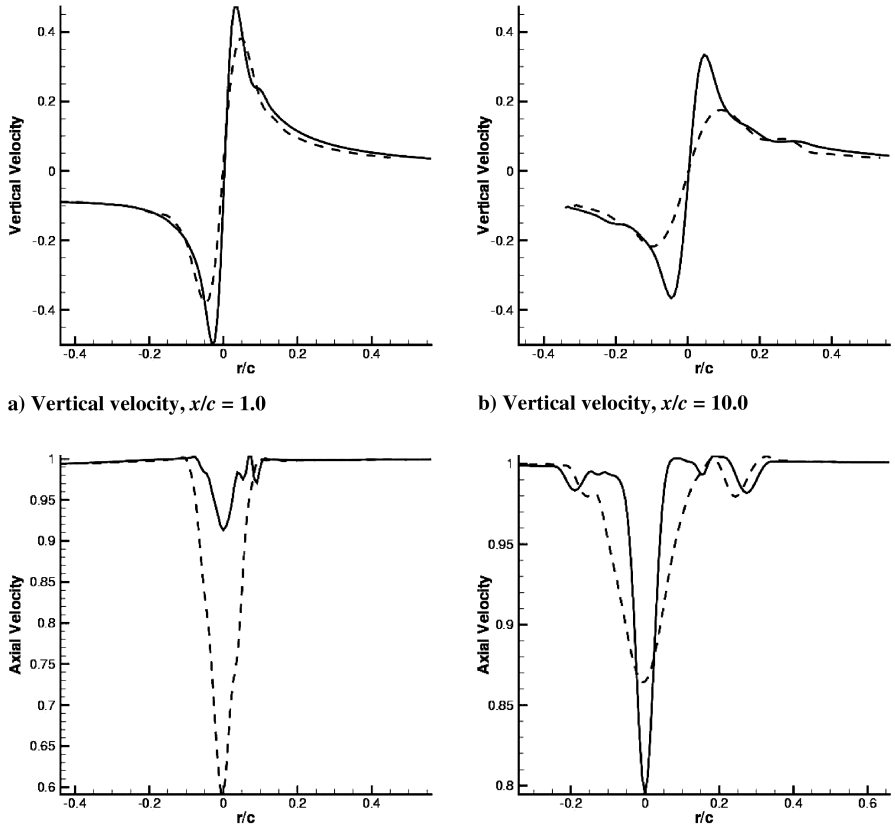


a) Vertical velocity, $x/c = 1.0$

b) Vertical velocity, $x/c = 10.0$

c) Axial velocity, $x/c = 1.0$

d) Axial velocity, $x/c = 10.0$

**Fig. 11 Comparison of baseline velocity profiles (solid lines) with blowing case C1 (dashed lines).**

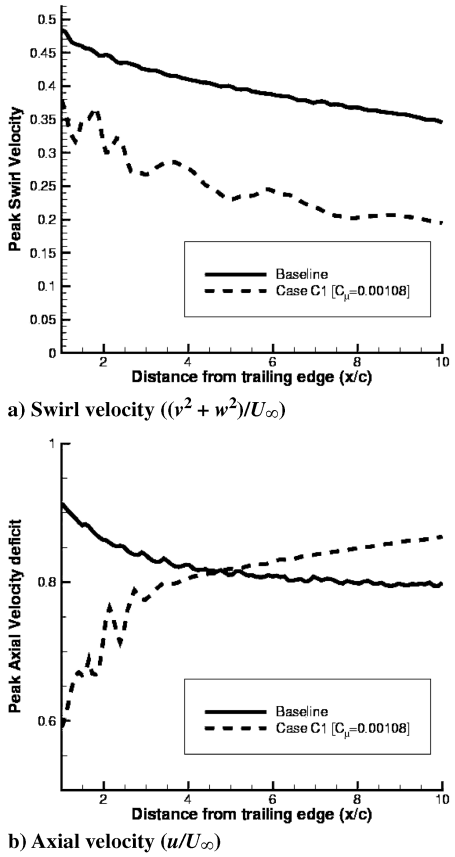


a) Swirl velocity ($(v^2 + w^2)/U_\infty$)

b) Axial velocity ($u/U_\infty$)

**Fig. 12 Comparison of baseline vortex evolution with blowing case C1.**

Beyond the downstream end of the jet, the large mass rate of flow from the lower surface is seen to tilt the vorticity vector and severely affect the axial component of vorticity (the result is seen in Fig. 14f). Remarkably, the rotational effects are strong enough, that by 1 chord downstream of the trailing edge, the tip vortex rolls up into a coherent form (Fig. 15a). However, as compared with the baseline case and blowing case C2 (Figs. 15b and 15c), the vortex structure for case C1 is not entirely axisymmetric since there seems to be an interaction with a region of counter-rotating vorticity.

As mentioned earlier, the decelerating effects of the interactions and axial shear cause the large axial momentum deficit.

As seen in Table 2, the blowing causes higher lift, evidently due to lower downwash velocities. Also, a larger drag force is noticed, which can be attributed to the high viscous losses and streamline disruption occurring during the interaction process.

*Effect of Jet Velocity*

Figure 16 shows the effect of blowing intensity on the vortex evolution. The reduction in swirl and axial velocities does not appear to be a linear function of the blowing intensity. As seen in Table 2, the lower blowing rates actually result in a larger $L/D$ efficiency, presumably due to the lower drag penalty.

*Effect of Jet Exit Angle*

No significant differences in the vortex structure or lift and drag were noticed for the $\theta_{\text{jet}} = \pm 15^\circ$ jet angle cases compared with the $\theta_{\text{jet}} = 0$ case.

## Conclusions

Practical RANS simulations of tip vortex formation and evolution suffer primarily from numerical diffusion errors and inaccurate turbulence modeling. In this work, the error due to numerical diffusion (which primarily arises from inadequate discretization of the nonlinear convective terms) is reduced by the use of proper grid

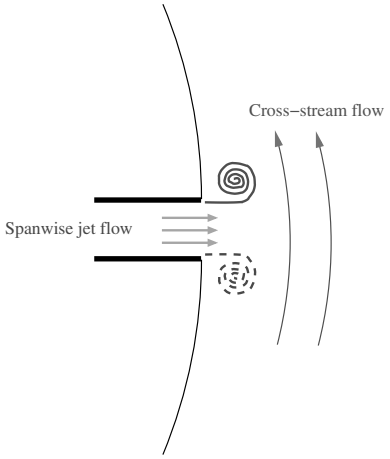


**Fig. 13 Schematic of formation of counter-rotating vortex pair in spanwise blowing.**

resolution (by means of grid clustering, orthogonality and overset meshes) and high order accurate numerical schemes. Turbulence modeling uncertainties were found to be minimized by adding a simple correction to the production term in the Spalart–Allmaras turbulence model. The fidelity of the approach allowed for a detailed study of the underlying physics of vortex formation and evolution. In addition, a strategy of vortex control, namely, spanwise blowing was evaluated.

1) With O(10–15) points per core length of discretization, and a smooth distribution of grid points, the current methodology is seen to give reasonable validation of mean flowfield velocities with experiments for two test cases that represent either end of a wide range of chord ($\mathrm{Re} = 2.2 \times 10^5$–$4.6 \times 10^6$) and vortex Reynolds numbers ($\mathrm{Re}_v \approx 8 \times 10^4$–$2 \times 10^6$).

2) Streamwise-oriented vorticity is developed by a *feeding sheet* comprising the crossflow boundary layer. Initial evidence of the tip vortex is seen when this boundary layer separates from the surface. The roll up of this separated boundary layer forms a system of vortices, which rapidly merge into a single coherent vortex.

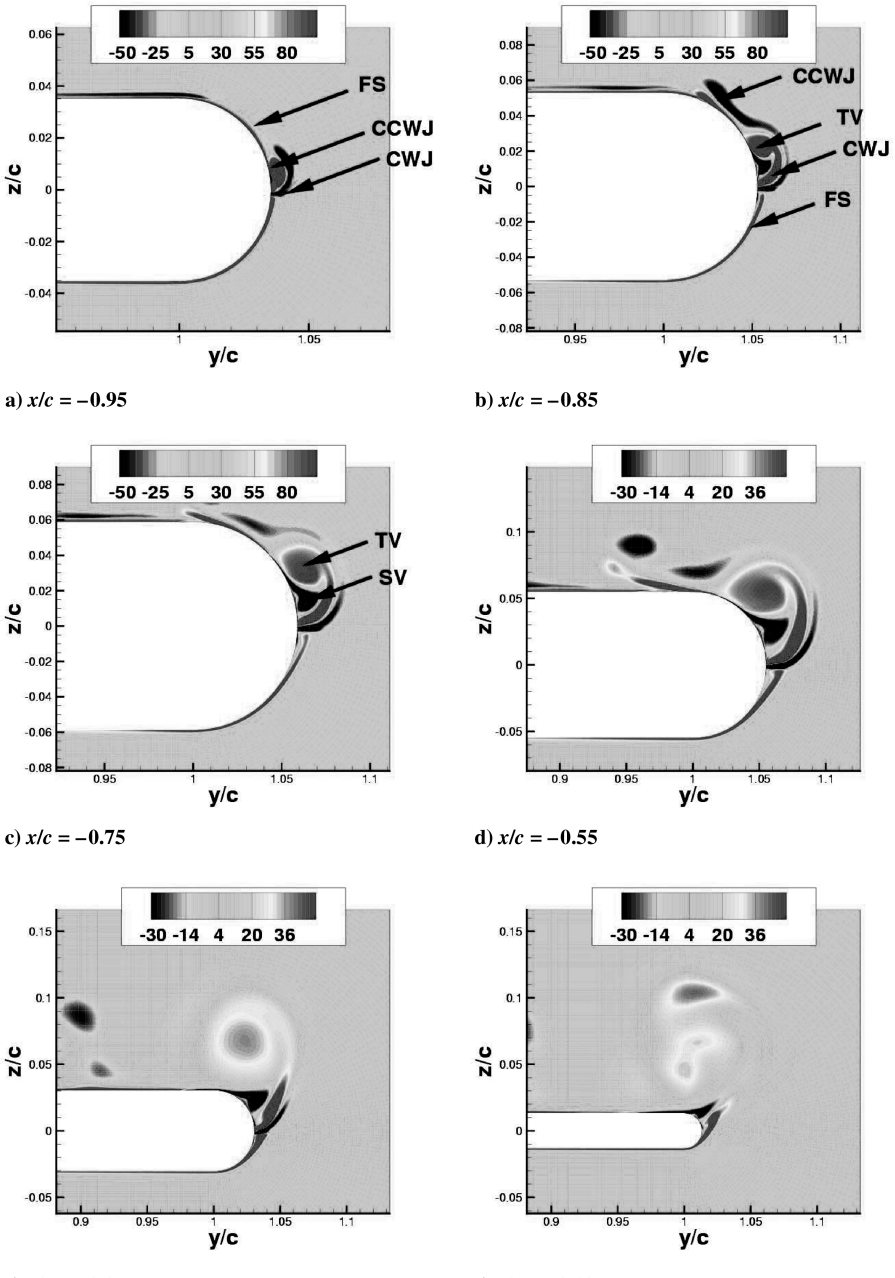


**a)** $x/c = -0.95$ **b)** $x/c = -0.85$

**c)** $x/c = -0.75$ **d)** $x/c = -0.55$

**e)** $x/c = -0.25$ **e)** $x/c = -0.10$

**Fig. 14 Axial vorticity evolution for blowing case C1. FS: Feeding sheet; CWJ: clockwise vorticity from spanwise jet; CCWJ: counterclockwise vorticity from spanwise jet; TV: tip vortex; SV: secondary vortex (counter-rotating to TV).**

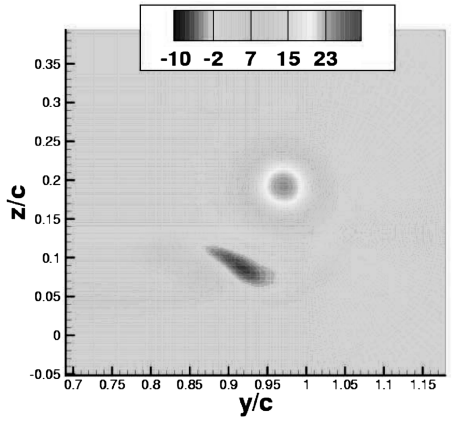


a) Blowing case C1

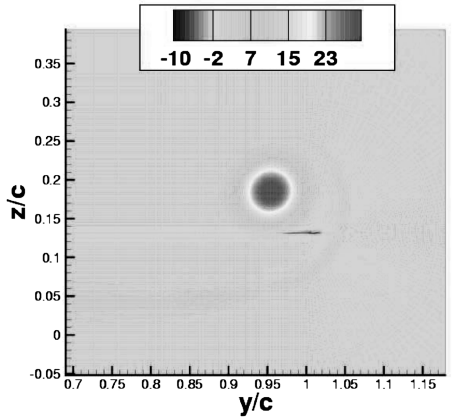


b) Blowing case C2

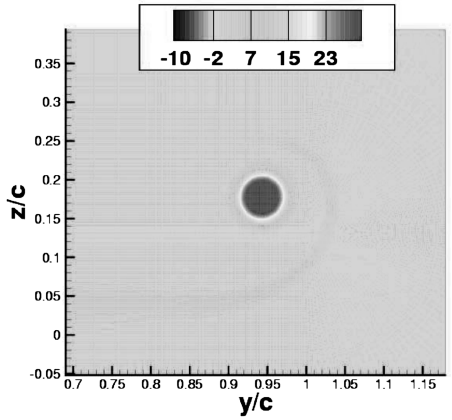


c) Baseline

**Fig. 15 Axial vorticity contours for baseline case and blowing cases C1, C2 at $x/c = 1.0$.**

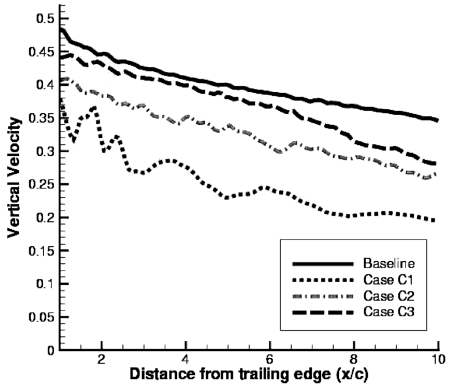


a) Peak swirl velocity

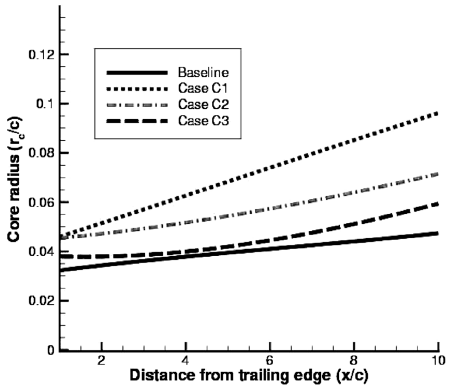


b) Core radius (curve-fit)

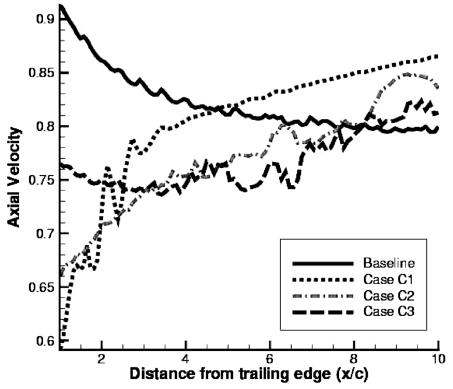


c) Peak axial velocity deficit

**Fig. 16 Effect of jet velocity on vortex evolution.**

3) The numerical validation of spanwise blowing with experimental velocity profile measurements showed good agreement.

4) The effect of spanwise blowing was to reduce the magnitude and development of the tangential momentum. The mechanism behind this effect appears to be the interaction of a pair of counter-rotating vortices generated at the jet exit with the feeding sheet of vorticity. This also results in a heightened axial velocity deficit, which also contributes to a radial transport of tangential momentum. The resulting tip vortex was found to be much more diffuse compared with the baseline case with no blowing.

5) Using moderate blowing ratios up to 30% reduction in peak swirl velocity was achieved with a marginal performance penalty. Although the details of the internal jet flow were not addressed, results suggest that concept holds promise as an effective vortex control strategy.

## Recommendations for Future Work

The extremely complicated nature of the flow, especially during the vortex formation is a prime example of nonequilibrium flow (such flows are characterized by multiple length scales and/or a significant imbalance between production and dissipation). In addition, streamline curvature and anisotropic effects [20] also seem to be important. Current day RANS models, especially linear eddy viscosity-based models, are not capable enough to address these issues in a comprehensive manner. Therefore, a primary suggestion for the continuation of this work would be to use the methodology with more advanced turbulence models such as the second moment closure (SMC) models. It has to be mentioned, however, that though SMC models have been demonstrated to be superior in some specific situations [31,36], they have not shown sustained improvement over the linear eddy viscosity models [37]. In addition, the complexity of these models and the associated computational stiffness has limited the range of their application.

When one considers real applications for spanwise blowing, it remains to be seen whether the current mass flow requirements are

practical. An alternative approach could be to bleed flow from the leading edge, as has been accomplished experimentally [26]. A more detailed study could involve using overset meshes to model the internal details of the bleeding process or even the plenum chamber in the experiment of [27].

## Acknowledgments

This work has been supported by the National Rotorcraft Technology Center under the Rotorcraft Centers of Excellence Program and was conducted at the Alfred Gessow Rotorcraft Center at the University of Maryland. The authors would like to thank Gregory Zilliac of the NASA Ames Research Center and Philippe Spalart of The Boeing Company for their help and suggestions.

## References

[1] Chow, J. S., Zilliac, G. G., and Bradshaw, P., "Mean and Turbulence Measurements in the Near Field of a Wingtip Vortex," *AIAA Journal*, Vol. 35, No. 10, 1997, pp. 1561–1567.

[2] Devenport, W. J., Rife, M. C., Liapis, S. I., and Follin, G. J., "The Structure and Development of a Wing-Tip Vortex," *Journal of Fluid Mechanics*, Vol. 312, 1996, pp. 71–104.

[3] Jacquin, L., and Pantano, C., "On the Persistence of Trailing Vortices," *Journal of Fluid Mechanics*, Vol. 471, 2002, pp. 159–168.

[4] Qin, J. H., "Numerical Simulations of a Turbulent Axial Vortex," Ph.D. Thesis, Department of Aerospace Engineering, Purdue University, 1998.

[5] Ragab, S., and Sreedhar, M., "Numerical Simulations of Vortices with Axial Velocity Deficits," *Physics of Fluids*, Vol. 7, No. 3, 1995, pp. 549–558.

[6] Moin, P., and Mahesh, K., "Direct Numerical Simulation: A Tool in Turbulence Research," *Annual Review of Fluid Mechanics*, Vol. 30, 1998, pp. 539–578.

[7] Piomelli, U., and Balaras, E., "Wall-Layer Models for Large-Eddy Simulations," *Annual Review of Fluid Mechanics*, Vol. 34, 2002, pp. 349–374.

[8] Hirsch, C., "Numerical Computation of Internal and External Flows," Vol. 1, Wiley, Chichester, England, 1988.

[9] Visbal, M. R., and Gaitonde, D. V., "On the Use of Higher-Order Finite-Difference Schemes on Curvilinear and Deforming Meshes," *Journal of Computational Physics*, Vol. 181, No. 1, 2002, pp. 155–185.

[10] Ekaterinaris, J. A., "High-Order Accurate, Low Numerical Diffusion Methods for Aerodynamics," *Progress in Aerospace Sciences*, Vol. 41, No. 3–4, 2005, pp. 192–300.

[11] Wake, B. E., and Choi, D., "Investigation of High-order Upwinded Differencing for Vortex Convection," *AIAA Journal*, Vol. 34, No. 2, 1996, pp. 332–337.

[12] Duraisamy, K., "Studies in Tip Vortex Formation, Evolution and Control," Ph.D. Thesis, Department of Aerospace Engineering, University of Maryland at College Park, 2005.

[13] Hall, C. M., and Long, L. N., "High Order Accurate Simulations of Wake and Tip Vortex Flowfields," *Proceedings of the 55th Annual Forum of the American Helicopter Society, Montreal, Canada, 1999* [CD-ROM].

[14] Dacles-Mariani, J., Kwak, D., and Zilliac, G., "On Numerical Errors and Turbulence Modeling in Tip Vortex Flow Prediction," *International Journal for Numerical Methods in Fluids*, Vol. 30, No. 1, 1999, pp. 65–82.

[15] Steinhoff, J., and Mersch, T., "Computation of Vortex Formation over ELAC-1 Configuration Using Vorticity Confinement," AIAA Paper 1995-6157, April 1995.

[16] Hariharan, N., and Sankar, L., "High-Order Essentially Nonoscillatory Schemes for Rotary-Wing Wake Computations," *Journal of Aircraft*, Vol. 41, No. 2, 2004, pp. 258–267.

[17] Lee, Y-L., and Baeder, J. D., "Vortex Tracking in Overset Method for Quad Tilt Rotor Blade Vortex Interaction," AIAA Paper 2003-3531, June 2003.

[18] Mansour, N. N., "Numerical Simulation of the Tip Vortex of a Low Aspect Ratio Wing at Transonic Speed," *AIAA Journal*, Vol. 23, No. 8, 1985, pp. 1143–1149.

[19] Srinivasan, G. R., McCroskey, W. J., Baeder, J. D., and Edwards, T. A., "Numerical Simulation of Tip Vortices of Wings in Subsonic and Transonic Flows," *AIAA Journal*, Vol. 26, No. 10, 1988, pp. 1153–1162.

[20] Dacles-Mariani, J., Zilliac, G. G., Chow, J. S., and Bradshaw, P. "Numerical/Experimental Study of a Wing Tip Vortex in the Near Field," *AIAA Journal*, Vol. 33, No. 9, 1995, pp. 1561–1568.

[21] Lockard, D. P., and Morris, P. J., "Wing-Tip Vortex Calculations Using a High-Accuracy Scheme," *Journal of Aircraft*, Vol. 35, No. 5, 1998, pp. 728–738.

[22] Spall, R. E., "Numerical Study of a Wing-Tip Vortex Using the Euler Equations," *Journal of Aircraft*, Vol. 38, No. 1, 2001, pp. 22–27.

[23] Egolf, T. A., "Recent Rotor Wake Simulation and Modeling Studies at United Technologies Corporation," AIAA Paper 2000-0115, Jan. 2000.

[24] Lee, C. S., Tavella, D., Wood, N. J., and Roberts, L., "Flow Structure and Scaling Laws in Lateral Wing-Tip Blowing," *AIAA Journal*, Vol. 27, No. 8, 1989, pp. 1002–1007.

[25] Mineck, R. E., "Study of Potential Aerodynamic Benefits From Spanwise Blowing at the Wing Tip," NASA TP-3515, 1995.

[26] Han, Y. O., and Leishman, J. G., "Experimental Investigation of Tip Vortex Alleviation Using a Slotted Tip Rotor Blade," *Proceedings of the 59th Annual Forum of the American Helicopter Society* [CD-ROM].

[27] Heyes, A. L., and Smith, D. A. R., "Spatial Perturbation of a Wing-Tip Vortex Using Pulsed Spanwise Jets," *Experiments in Fluids*, Vol. 37, No. 1, 2004, pp. 120–127.

[28] Shu, C.-W., "High-Order Finite Difference and Finite Vol. WENO Schemes and Discontinuous Galerkin Methods for CFD," *International Journal of Computational Fluid Dynamics*, Vol. 17, No. 2, 2003, pp. 107–118.

[29] Huynh, H. T., "Accurate Monotone Cubic Interpolation," *SIAM Journal on Numerical Analysis*, Vol. 30, 1993, pp. 57–100.

[30] Spalart, P. R., and Allmaras, S. R., "A One-Equation Turbulence Model for Aerodynamic Flows," AIAA Paper 92-0439, June 1992.

[31] Jakirlic, S., Hanjalic, K., and Tropea, C., "Modeling Rotating and Swirling Turbulent Flows: A Perpetual Challenge," *AIAA Journal*, Vol. 40, No. 10, 2002, pp. 1984–1996.

[32] Martin, P. B., Pugilese, G. J., and Leishman, J. G., "High Resolution Trailing Vortex Measurements in the Wake of a Hovering Rotor," *Proceedings of the 53rd Annual Forum of the American Helicopter Society* [CD-ROM].

[33] Batchelor, G. K., "Axial Flow in Trailing Line Vortices," *Journal of Fluid Mechanics*, Vol. 20, 1964, pp. 645–658.

[34] Uberoi, M. S., "Mechanisms of Decay of Laminar and Turbulent Vortices," *Journal of Fluid Mechanics*, Vol. 92, No. 2, 1979, pp. 241–255.

[35] Fabre, D., and Jacquin, L., "Viscous Instabilities in Trailing Vortices at Large Swirl Numbers," *Journal of Fluid Mechanics*, Vol. 500, 2004, pp. 239–256.

[36] Gatski, T. B., and Speziale, C. G., "On Explicit Algebraic Stress Models for Complex Turbulent Flows," *Journal of Fluid Mechanics*, Vol. 254, 1993, pp. 59–75.

[37] Spalart, P. R., "Trends in Turbulence Treatments," AIAA Paper 2000-2306, June 2000.